Investigation of nonlinear control of galloping with a linear beam with elastic boundary conditions

Matthieu Leroux, Sébastien Langlois, Alireza Ture Savadkoohi

Investigation of nonlinear control of galloping with a linear beam with elastic boundary conditions

M. Leroux[a,*], S. Langlois[b], A. Ture Savadkoohi[a]

[a] *Univ Lyon, ENTPE, Ecole Centrale de Lyon, CNRS, LTDS, UMR5513, 69518 Vaulx-en-Velin, France*
[b] *University of Sherbrooke, 2500 Bd de l'Université, Sherbrooke, QC J1K 2R1, Canada*

Abstract

The aim of this study is nonlinear passive control of galloping oscillation on overhead transmission lines. The considered system is a linear beam subjected to harmonic and aerodynamic excitations which is coupled to a nonlinear absorber placed on an arbitrary position along the beam. Both extremities of the beam present rotationally and translationally elastic boundary conditions. After projection of spatio-temporal equations of the system on an arbitrary mode of the beam (the mode to be controlled), fast and slow system dynamics are traced which predict periodic or non periodic regimes. All analytical developments are compared with numerical results obtained from direct numerical integration of system equations and also from finite element modelling of the overall structure. Then, nonlinear passive control process of galloping instability by a non smooth nonlinear energy sink (NES) is investigated on a real case of galloping instability on a transmission line cable due to accretion of ice on it.

Keywords:
Beam, elastic boundary conditions, transmission line, galloping, nonlinear passive control, nonlinear energy sink, fast/slow dynamics, finite element model

1. Introduction

Control problems in civil and mechanical engineering systems covered large spectrum ranging from active to passive control [1], [2], [3]. Active control solutions need external energies for the activations while passive control strategies rely on interactions between coupled oscillators or systems for energy reductions. Passive controllers are divided into two categories: linear and nonlinear systems. For linear passive controllers, their restoring forcing function reads as $\mathcal{F}(\alpha) = k_L\alpha$ where α stands for generalized displacement. The most famous passive control device is the Frahm system [4] which is named also a tuned

*Corresponding author-matthieu.leroux@entpe.fr

mass damper (TMD) [5]. Such linear systems are very efficient at the targeted frequency but they lose their efficiencies elsewhere notably for large frequency bands. Roberson [6] supplemented the linear part of the absorber by a cubic term reading as $\mathcal{F}(\alpha) = k_L\alpha + k_{NL}\alpha^3$. He showed that the working frequency of such absorbers increases with respect to the TMD. Since then, different types of nonlinear absorbers were introduced: pendulum-type vibration absorbers [7], [8], auto parametric vibration absorber [9],[10],[11], magnet type nonlinear absorber [12],[13], softening type nonlinear absorber [14], bow-type or shallow buckled beam [15].

In the early 21st century a new type of nonlinear absorber has been developed which contained pure cubic term reading as $\mathcal{F}(\alpha) = k_{NL}\alpha^3$ [16], [17], [18]. It was named a nonlinear energy sink (NES). The NES has no special frequency and can enter in resonance at any frequency. It is shown that the control process by NES is functional for large frequency bands. Different types of nonlinearities are considered for the NES: vibro-impact NES [19],[20],[21],[22], piecewise linear NES [23]. The NES has been applied successfully in different systems covering aerospace [24], mechanical [25], civil [26] and acoustical [27],[28] engineering.

Galloping oscillations on overhead power lines are a major issue, as they correspond to large amplitudes at low-frequencies. They are caused by ice and snow accretion on conductor cables [29]. The galloping instability was first studied by Den Hartog that gave his theory on its vertical mechanism [30]. Since then, numerous studies have studies the galloping mechanism with the consideration of the coupling of the different types of motions of the cable [31], [32], [33]. Recent work has examined a continuous cable model under galloping instability which points out the different internal resonances [34]. A lack of control solutions remains even if there are some widely used techniques to deal with galloping oscillations. The interphase spacer [29] is a device designed to keep a clearance between different phases of an electric circuit. Most of the studies on interphase spacers concentrate on the optimization of the location of the device along the span concerning galloping mitigation [35]. The torsional pendulum is a small eccentric mass attached to the conductor to modify the coupling between the vertical and the torsional motion of the cable [36]. There are several categories of vibrations which demand different control strategy, for example aeolian vibration can be mitigated by a tuned mass damper [37].

Beam-like structural elements have many applications in different engineering systems such as the wing of an airplane, the overall behaviour of homogenized tall buildings, a simple model of the bridge deck, etc. The control process of such elements with classical boundary conditions by cubic NES has been articulated in [38], [39], [40]. In this paper, we propose the control strategy of a linear beam with elastic boundary conditions (translational and rotational springs) by considering a general form of nonlinearity for the restoring forcing function of the NES, narrowed later on non-smooth nonlinearity, for numerical applications. The linear beam with elastic boundary conditions have been chosen to study the soft structures under aerodynamic instability as a cable of overhead transmission line with ice-accretion. In addition the studied system is very similar to an experimental test on galloping instability of overhead transmission line by

Chabart et al. [41], and the aerodynamic coefficients of this reference will be used here to model the aerodynamic effects.
The organization of the paper is as follows: the global representation of the system under two different types of excitation coupled to a NES with a general nonlinearity is presented in section 2. The primary treatments of system equations are presented in the same section. Fast and slow system dynamics are detected in section 3, then section 4 presents the numerical validation by the finite element method. In section 5 the nonlinear passive control of the system submitted to galloping instability is investigated. Finally, the paper is concluded in section 6.

2. Formulation of the problem

The system under consideration is a linear beam with elastic boundary conditions, considered as the principal system, coupled to a NES at $x = l_n$, as it is illustrated on Fig. 1. The principal system is an Euler-Bernoulli beam characterized by a flexural stiffness EI, a length L, a linear mass density $m(x)$ considered to be constant all along the beam. Its boundary conditions are defined by translational and rotational stiffnesses. Translation and rotational stiffnesses of boundary conditions at $x = 0$, $x = L$ are represented by (k_0 and k_{R0}) and (k_L and k_{RL}) respectively. The motion of the beam is represented by $v(x,t)$ which is the vertical displacement between the equilibrium state and the actual configuration. The NES is composed of a small mass m_{NES}, a nonlinear stiffness defined by a nonlinear restoring function $\mathcal{F}$, and a viscous damping c_{NES}. The motion of the NES is characterized by $u(t)$ which is the vertical displacement between the equilibrium position and the actual configuration.

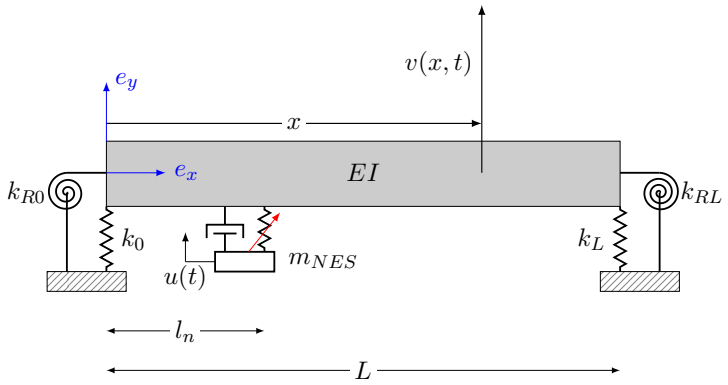

Figure 1: The system under consideration: The linear Euler-Bernoulli beam with the length of L and elastic boundary conditions is coupled to a NES at $x = l_n$.

In the next section, we will evaluate different mode shapes Φ_n and frequencies ω_n of the principal system.

2.1. Modal characteristics of the system

The equation of motion of the conservative beam reads as:

$$-EI\frac{\partial^4 v}{\partial x^4}(x,t) = m(x)\frac{\partial^2 v}{\partial t^2}(x,t) \tag{1}$$

With the following boundary conditions:

$$\text{At} \quad x=0 \quad : \begin{cases} k_0 v(0,t) = -EI\dfrac{\partial^3 v}{\partial x^3}(0,t) \\ EI\dfrac{\partial^2 v}{\partial x^2}(0,t) = k_{R0}\dfrac{\partial v}{\partial x}(0,t) \end{cases} \tag{2}$$

$$\text{At} \quad x=L \quad : \begin{cases} k_L v(L,t) = EI\dfrac{\partial^3 v}{\partial x^3}(L,t) \\ EI\dfrac{\partial^2 v}{\partial x^2}(L,t) = -k_{RL}\dfrac{\partial v}{\partial x}(L,t) \end{cases} \tag{3}$$

After separation of spatiotemporal variable as $v(x,t) = \Phi(x)F(t)$, Eq. 1 leads to:

$$\frac{\mathrm{d}^2\mathrm{F}}{\mathrm{dt}^2}(t) + \omega^2 F(t) = 0 \tag{4}$$

$$\frac{\mathrm{d}^4\Phi}{\mathrm{dx}^4}(x) - \beta^4\Phi(x) = 0 \quad \text{with} \quad \beta^4 = \frac{m}{EI}\omega^2 \tag{5}$$

To respect the finite motion property of the non-excited system, the constant ω has to be positive. The solutions of the differential equations Eq. 4 and 5 can be written depending on constants a_0, a_1, a_2, a_3, a_4 and θ_0 as:

$$F(t) = a_0\cos(\omega t + \theta_0) \tag{6}$$

$$\Phi(x) = a_1\sin(\beta x) + a_2\cos(\beta x) + a_3\cosh(\beta x) + a_4\sinh(\beta x) \tag{7}$$

Then the mathematical expression of the boundary conditions defined in Eq. 2 and Eq. 3 can be rewritten in the matrix form as:

$$M\begin{bmatrix} a_1 \\ a_2 \\ a_3 \\ a_4 \end{bmatrix} = \begin{bmatrix} 0 \\ 0 \\ 0 \\ 0 \end{bmatrix} \tag{8}$$

M is a 4×4 matrix which is presented in Appendix A. The non-trivial solutions of Eq. 8 exist if the matrix M is non-invertible. The solutions of $\det(M) = 0$ lead to the determination of the natural frequencies which should be obtained numerically. Then, constants a_1, a_2, a_3 and a_4 can be determined. The details of all calculations are provided in Appendix A. The proof of orthogonality of modes for considered boundary conditions is provided in Appendix B. Finally, the normalized mode shapes can be defined by:

$$\int_0^L m(x)\Phi_i^2(x)\mathrm{dx} = 1 \tag{9}$$

2.2. Projection of the system on one of its modes

Let us suppose that the overall system is under a distributed force $f_a(x,t)$ that only sollicitate one of the natural modes of the principal system. Consequently, we will study the mono-modal dynamics of the system. The general dynamic equation of the beam can be written as: :

$$-EI\frac{\partial^4 v}{\partial x^4}(x,t) + f(x,t) = m\frac{\partial^2 v}{\partial t^2}(x,t) + C\frac{\partial v}{\partial t}(x,t) \tag{10}$$

Where C is the linear viscous damping and $f(x,t)$ stands for the applied reactions along the beam. The restoring force function of the NES is defined by the function $\mathcal{F}$. So,

$$\begin{aligned} f(x,t) = \quad & -c_{NES}\left(\frac{\partial v}{\partial t}(l_n,t) - \frac{\partial u}{\partial t}(t)\right)\delta(x-l_n) \\ & -\mathcal{F}(v(l_n,t)-u(t))\delta(x-l_n) + f_a(x,t) \end{aligned} \tag{11}$$

The dynamic equilibrium of the NES reads:

$$m_{NES}\frac{\partial^2 u}{\partial t^2}(t) + c_{NES}\left(\frac{\partial u}{\partial t}(t) - \frac{\partial v}{\partial t}(l_n,t)\right) - \mathcal{F}(v(l_n,t)-u(t)) = 0 \tag{12}$$

The excitation is assumed to mainly bring the k^{th} natural frequency. Moreover, we assume that for this case the response of the system are governed only by the k^{th} mode. So, we set:

$$v(x,t) = q_k(t)\Phi_k(x) \tag{13}$$

The system equations are projected on the k^{th} mode which yield to:

$$\begin{aligned} & -EIq_k\beta_1 - c_{NES}\left(\frac{\partial q_k}{\partial t}\Phi_k(l_n) - \frac{\partial u}{\partial t}\right)\Phi_k(l_n) - \mathcal{F}\left(q_k\Phi_k(l_n) - u\right)\Phi_k(l_n) \\ & + \int_0^L f_a(x,t)\Phi_k(x)\mathrm{d}x = m\frac{\partial^2 q_k}{\partial t^2}\beta_2 + C\frac{\partial q_k}{\partial t}\beta_2 \end{aligned} \tag{14}$$

$$m_{NES}\frac{\partial^2 u}{\partial t^2}(t) + c_{NES}\left(\frac{\partial u}{\partial t}(t) - \frac{\partial q_k}{\partial t}\Phi_k(l_n)\right) - \mathcal{F}(q_k\Phi_k(l_n) - u(t)) = 0 \tag{15}$$

Where,

$$\begin{aligned} \beta_1 &= \int_0^L \frac{\partial^4 \Phi_k}{\partial x^4}\Phi_k dx \\ \beta_2 &= \int_0^L \Phi_k^2 dx \end{aligned} \tag{16}$$

The mass of the NES is considered very small compared to the one of the primary system i.e. $\epsilon = \dfrac{m_{NES}}{mL} \ll 1$. We introduce the following non-dimensionalized space and time variables:

$$\bar{x} = \frac{x}{L} \tag{17}$$

$$\tau = \omega_k t \quad \text{with,} \quad \omega_k^2 = \frac{EI}{m}\frac{\beta_1}{\beta_2} \tag{18}$$

Then, Eqs. 14 and 15 read:

$$\ddot{p}_k(\tau) + \epsilon C_p \dot{p}_k + p_k(\tau) + \epsilon\alpha c\left(\dot{p}_k(\tau) - \dot{\bar{u}}(\tau)\right) + \epsilon\alpha\bar{\mathcal{F}}\left(p_k(\tau) - \bar{u}(\tau)\right) = \epsilon\Gamma(\tau) \tag{19}$$

$$\epsilon\ddot{\bar{u}}(\tau) + \epsilon c\left(\dot{\bar{u}}(\tau) - \dot{p}_k(\tau)\right) - \epsilon\bar{\mathcal{F}}\left(p_k(\tau) - \bar{u}(\tau)\right) = 0 \tag{20}$$

Where $\dot{()} = \dfrac{\mathrm{d}}{\mathrm{d}\tau}()$. System parameters are reported in Appendix C. In the next section, we will study the nonlinear equations with a multiple-scale method [42].

2.3. Harmonic excitation

The first type of external excitation is composed of two nodal vertical sinusoidal forces at both ends of the beam. The two forces are set with the same frequency and the same phase. The distributed force f_a can be expressed as:

$$f_a(x,t) = F_1 \sin(\Omega_r t)\delta(x) + F_2 \sin(\Omega_r t)\delta(x - L) \tag{21}$$

With F_1, F_2, Ω_r, and δ the amplitudes of the forces, the angular frequency of the forces and the Dirac function. In this case, the force term in the discrete non-dimensional equation can be developed as:

$$\epsilon\Gamma = \frac{L^2\bar{\Phi}_k\left(\frac{l_n}{L}\right)}{EI\bar{\beta}_1}\left(F_1\bar{\Phi}_k(0) + F_2\bar{\Phi}_k(1)\right)\sin\left(\frac{\Omega_r}{\omega_k}\tau\right) \tag{22}$$

Then the parameters γ and Ω are introduced to simplify the mathematical developments.

$$\Gamma = \gamma\sin(\Omega\tau) \tag{23}$$

With,

$$\gamma = \frac{L^2\bar{\Phi}_k\left(\frac{l_n}{L}\right)}{\epsilon EI\bar{\beta}_1}\left(F_1\bar{\Phi}_k(0) + F_2\bar{\Phi}_k(1)\right) \tag{24}$$

And,

$$\Omega = \frac{\Omega_r}{\omega_k} \tag{25}$$

2.4. Aerodynamic excitation

The galloping phenomenon results from the wind-structure interaction. The quasi-steady theory introduced by Den Hartog [30] is used here to evaluate the vertical forces induced by the wind on the beam with ice accretion. According to this theory, when the beam is moving in the vertical direction, the dynamic forces caused by a horizontal wind are assumed to be equal to the static forces caused by the relative wind. The relative wind is the initial wind (characterized by its angle of attack and magnitude) with a modified magnitude and angle of

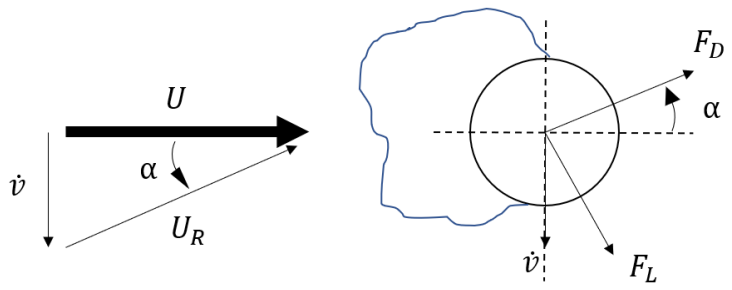

Figure 2: Dynamic forces on a beam with circular cross-section and ice-accretion where $\dot{v}$, U, U_R, α, F_L, and F_D are the vertical speed of the beam, the real wind speed, the relative wind speed, the relative angle of attack, the lift force and the drag force.

attack depending on the vertical velocity of the section as it is shown in figure 2.

The angle of attack, α, is defined as:

$$\alpha = \tan\left(\frac{\dot{v}}{U}\right) \tag{26}$$

The wind speed U_R is defined as:

$$U_R^2 = U^2 + \dot{v}^2 \tag{27}$$

Then the distributed force reads:

$$f_a(x,t) = -F_D(\alpha(x,t))\sin(\alpha(x,t)) + F_L(\alpha(x,t))\cos(\alpha(x,t)) \tag{28}$$

The drag and the lift forces are expressed as:

$$\begin{aligned} F_D &= \frac{1}{2}\rho_f b U_R^2 C_D(\alpha(x,t)) \\ F_L &= \frac{1}{2}\rho_f b U_R^2 C_L(\alpha(x,t)) \end{aligned} \tag{29}$$

With ρ_f, b, C_D, and C_L the density of air, the diameter of the beam with ice-accretion, the drag coefficient, and the lift coefficient. Finally, we can consider a polynomial development up to the order three of the force f_a:

$$f_a(x,t) = \frac{1}{2}\rho_f b U^2 \left(A_0 - A_1\frac{\dot{v}}{U} - A_2\left(\frac{\dot{v}}{U}\right)^2 - A_3\left(\frac{\dot{v}}{U}\right)^3\right) \tag{30}$$

The coefficients of the distributed force can be calculated with the drag and the lift coefficients at each angle of attack. Chabart [41] performed aerodynamic and aeroelastic tests on a piece of cable with ice accretion. The data on the lift and the drag coefficients of reference [41] will be used to calculate the coefficient

of the distributed force. Those coefficient are shown on the figure 3, where $\tilde{f}_a$ can be written as:

$$\tilde{f}_a = -C_D(\alpha(x,t))\sin(\alpha(x,t)) + C_L(\alpha(x,t))\cos(\alpha(x,t)) \tag{31}$$

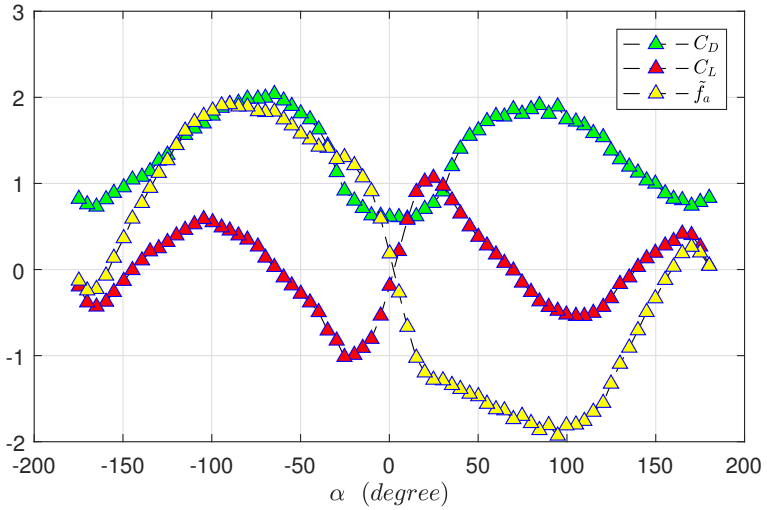

Figure 3: The aerodynamic coefficients of the beam cross section with ice-accretion and the force coefficient $\tilde{f}_a$ vs. angle of attack.

Then, the $\Gamma(t)$ function in Eq. 19 yields to :

$$\Gamma = \alpha_0 - \alpha_1\dot{p}_k - \alpha_2\dot{p}_k^2 - \alpha_3\dot{p}_k^3 \tag{32}$$

With,

$$\begin{aligned}
\epsilon\alpha_0 &= \frac{\bar{\Phi}_k\left(\frac{l_n}{L}\right)\rho_f U^2 b A_0}{2mL\bar{\beta}_2\omega_k^2}\int_0^1 \bar{\Phi}_k \mathrm{d}\bar{x} \\
\epsilon\alpha_1 &= \frac{\rho_f b U A_1}{2m\omega_k} \\
\epsilon\alpha_2 &= \frac{\rho_f b A_2 L}{2m\bar{\beta}_2\bar{\Phi}_k\left(\frac{l_n}{L}\right)}\int_0^1 \bar{\Phi}_k^3 \mathrm{d}\bar{x} \\
\epsilon\alpha_3 &= \frac{\rho_f b A_3 L^2\omega_k}{2m\bar{\beta}_2 U\bar{\Phi}_k\left(\frac{l_n}{L}\right)}\int_0^1 \bar{\Phi}_k^4 \mathrm{d}\bar{x}
\end{aligned} \tag{33}$$

3. General methodology used for detection of different system dynamics

The dynamic equations of the system are nonlinear due to the nonlinearity of the restoring force function $\mathcal{F}$. To point out some characteristics of the system, we will reduce the order of the system by using complex variables of Manevitch [43]. We will study the system at different time scales [42].

3.1. Complexification

Let us introduce new variables standing for displacement of the center of the mass of the system (w) and the relative displacement between the principal system and the NES (v):

$$\begin{aligned} w &= \frac{m_{NES}\bar{u} + mLp_k}{m_{NES} + mL} \approx p_k + \epsilon\bar{u} \\ v &= p_k - \bar{u} \end{aligned} \tag{34}$$

Let us introduce Ω the angular frequency corresponding to the response of the system. As we are interested to study the system behaviors around a 1:1 resonance (with the mode k), we set $\Omega = 1 + \epsilon\sigma$. Equations 19 and 20 with the new variables read as:

$$\ddot{w} + w + \epsilon v + \epsilon(\alpha - 1)\bar{\mathcal{F}}(v) + \epsilon c(\alpha - 1)\dot{v} + \epsilon C_p(\dot{w} + \epsilon\dot{v}) = \epsilon\Gamma \tag{35}$$

$$\ddot{v} + w + \epsilon v + (\epsilon\alpha + 1)\bar{\mathcal{F}}(v) + c(\epsilon\alpha + 1)\dot{v} + \epsilon C_p(\dot{w} + \epsilon\dot{v}) = \epsilon\Gamma \tag{36}$$

The complex variables of Manevitch [43] are introduced as (with $i^2 = -1$):

$$\begin{cases} \varphi_1 e^{i\Omega\tau} = \dot{w} + i\Omega w \\ \varphi_2 e^{i\Omega\tau} = \dot{v} + i\Omega v \end{cases} \tag{37}$$

These variables are injected in Eqs. 35 and 36 and only the first harmonics are kept by a Galerkin method. If $\Lambda(\varphi_1, \varphi_2, \varphi_1^*, \varphi_2^*)$ is a general function, the first harmonic λ is obtained via:

$$\lambda(\varphi_1, \varphi_2, \varphi_1^*, \varphi_2^*) = \frac{\Omega}{2\pi}\int_0^{\frac{2\pi}{\Omega}} \Lambda(\varphi_1, \varphi_2, \varphi_1^*, \varphi_2^*)e^{-i\Omega\tau}\mathrm{d}\tau \tag{38}$$

We assume that the functions φ_1 and φ_2 do not depend on τ. This will be validated during the multiple scale method, or we will look at system behaviors at the infinity of the fast time. After keeping only the first harmonic, the Eqs. 35 and 36 becomes:

$$\begin{aligned} &\dot{\varphi_1} - \frac{\Omega}{2i}\varphi_1 + \frac{1}{2i\Omega}(\varphi_1 + \epsilon\varphi_2) + \epsilon(\alpha - 1)\frac{\varphi_2}{2i\Omega}G(|\varphi_2|^2) + \frac{\epsilon c(\alpha - 1)}{2}\varphi_2 \\ &+ \frac{\epsilon C_p}{2}(\varphi_1 + \epsilon\varphi_2) = \epsilon\Gamma_1 \end{aligned} \tag{39}$$

$$\begin{aligned} &\dot{\varphi_2} - \frac{\Omega}{2i}\varphi_2 + \frac{1}{2i\Omega}(\varphi_1 + \epsilon\varphi_2) + (\epsilon\alpha + 1)\frac{\varphi_2}{2i\Omega}G(|\varphi_2|^2) + \frac{c(\epsilon\alpha + 1)}{2}\varphi_2 \\ &+ \frac{\epsilon C_p}{2}(\varphi_1 + \epsilon\varphi_2) = \epsilon\Gamma_1 \end{aligned} \tag{40}$$

With Γ_1 the first harmonic terms of Γ and the function G defined as:

$$G(|\varphi_2|^2) = \frac{2i\Omega}{\varphi_2}\frac{\Omega}{2\pi}\int_0^{\frac{2\pi}{\Omega}} \bar{\mathcal{F}}\left(\frac{\varphi_2 e^{i\Omega\tau} - \varphi_2^* e^{-i\Omega\tau}}{2i\Omega}\right)e^{-i\Omega\tau}\mathrm{d}\tau \tag{41}$$

For the detection of different dynamics of the system, the method of multiple scales [42] is used. Different times scales τ_n are introduced, $\tau_n = \epsilon^n \tau$, with $n \in \mathbb{N}$. Eqs. 39 and 40 can be extended in series concerning ϵ and the terms in the same order should be treated separately. The function G is extended in series as:

$$G = G_0 + \epsilon G_1 + \mathcal{O}(\epsilon^2) \tag{42}$$

Here, the non-smooth NES is defined by its restoring force function that is piecewise linear. Figure 4 shows its restoring force function depending on K_1, K_2, the two slopes of the function, and the clearance 2δ standing for the position where the slope changes. This function is defined as:

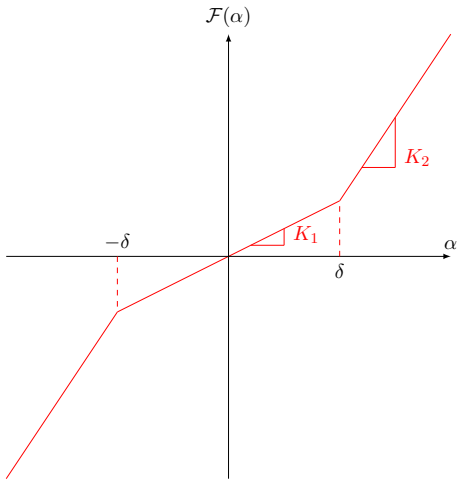

Figure 4: The restoring forcing function of considered non-smooth NES.

$$\mathcal{F}(\alpha) = \begin{cases} K_1\alpha & \text{if} \quad \alpha \in [-\delta, \delta] \\ K_2\alpha + \delta(K_1 - K_2) & \text{if} \quad \alpha > \delta \\ K_2\alpha + \delta(K_2 - K_1) & \text{if} \quad \alpha < -\delta \end{cases} \tag{43}$$

The non-dimensional restoring force function $\bar{\mathcal{F}}$ that was defined in section 2 reads:

$$\bar{\mathcal{F}}(\alpha) = \begin{cases} k_1\alpha & \text{if} \quad \alpha \in [-\bar{\delta}, \bar{\delta}] \\ k_2\alpha + \bar{\delta}(k_1 - k_2) & \text{if} \quad \alpha > \bar{\delta} \\ k_2\alpha + \bar{\delta}(k_2 - k_1) & \text{if} \quad \alpha < -\bar{\delta} \end{cases} \tag{44}$$

With,

$$\bar{\delta} = \frac{\delta}{L} \quad ; \quad \epsilon k_1 = \frac{K_1 L^3}{EI} \quad ; \quad \epsilon k_2 = \frac{K_2 L^3}{EI} \tag{45}$$

The function G (see Eq. 41) is defined as:

$$G(|\varphi_2|^2) = \begin{cases} k_1 & \text{if} \quad \dfrac{|\varphi_2|}{\Omega} \leq \bar{\delta} \\ g(|\varphi_2|^2) & \text{else} \end{cases} \tag{46}$$

Where,

$$\begin{aligned} g(|\varphi_2|^2) = \quad & \frac{2\bar{\delta}\Omega}{N_2^2\pi}(k_1-k_2)\sqrt{N_2^2-\bar{\delta}^2\Omega^2} \\ & +\frac{2}{\pi}\left(k_2\arccos\left(\frac{\bar{\delta}\Omega}{N_2}\right)+k_1\arcsin\left(\frac{\bar{\delta}\Omega}{N_2}\right)\right) \end{aligned} \tag{47}$$

Then the $\mathcal{O}(\epsilon^0)$ of the function G can be calculated.

$$G_0(|\varphi_2|^2) = \begin{cases} k_1 & \text{if} \quad |\varphi_2| \leq \bar{\delta} \\ g_0(|\varphi_2|^2) & \text{else} \end{cases} \tag{48}$$

$$\begin{aligned} g_0(|\varphi_2|^2) = \quad & \frac{2\bar{\delta}}{N_2^2\pi}(k_1-k_2)\sqrt{N_2^2-\bar{\delta}^2} \\ & +\frac{2}{\pi}\left(k_2\arccos\left(\frac{\bar{\delta}}{N_2}\right)+k_1\arcsin\left(\frac{\bar{\delta}}{N_2}\right)\right) \end{aligned} \tag{49}$$

In the following sections, different system dynamics will be detected by studying the system at different orders of ϵ.

3.2. Fast dynamics of the system

In the previous section, the truncated forms of the system equations are presented (Eqs. 39 and 40). The $\mathcal{O}(\epsilon^0)$ of these equations reads:

$$\begin{cases} \dfrac{\partial\varphi_1}{\partial\tau_0}-\dfrac{\varphi_1}{2i}+\dfrac{\varphi_1}{2i}=0 \\ \dfrac{\partial\varphi_2}{\partial\tau_0}-\dfrac{\varphi_2}{2i}+\dfrac{\varphi_1}{2i}+\dfrac{\varphi_2 G_0(|\varphi_2|^2)}{2i}+\dfrac{c}{2}\varphi_2=0 \end{cases} \tag{50}$$

The first equation gives $\dfrac{\partial\varphi_1}{\partial\tau_0}=0$. Let us seek fixed points of the system. This means that when $\tau_0\to\infty$, then $\dfrac{\partial\varphi_2}{\partial\tau_0}=0$. Then, the second equation of 50 provides:

$$\mathscr{H}(\varphi_1,\varphi_2,\varphi_1^*,\varphi_2^*)=0 \tag{51}$$

With,

$$\mathscr{H}=\frac{\varphi_1}{2i}-\frac{\varphi_2}{2i}+\frac{\varphi_2 G_0(|\varphi_2|^2)}{2i}+\frac{c}{2}\varphi_2 \tag{52}$$

$\mathscr{H}$ is named Slow Invariant Manifold (SIM) in the complex domain. As φ_1 and φ_2 are complex variables, we set $\varphi_j=N_j e^{i\delta_j}$ with $j=1,2$, $N_j\in\mathbb{R}^+$, $\delta_j\in\mathbb{R}$. By separating the real parts and the imaginary parts of $\mathscr{H}$ following relation is obtained:

$$N_1=N_2\sqrt{c^2+\left(1-G_0(N_2^2)\right)^2} \tag{53}$$

Equation 53 is the representation of the SIM in the real domain, it collects all equilibrium points that the system can reach. To perform a stability analysis of

the SIM, we linearly perturb φ_2 (respectively φ_2^*) as $\varphi_2+\Delta\varphi_2$ with $|\Delta\varphi_2| \ll |\varphi_2|$ (respectively $\varphi_2^* + \Delta\varphi_2^*$ with $|\Delta\varphi_2^*| \ll |\varphi_2^*|$). The Eq. 50 rewrites as:

$$\begin{array}{l} \frac{\partial(\varphi_2+\Delta\varphi_2)}{\partial\tau_0} - \frac{1}{2i}(\varphi_2+\Delta\varphi_2) + \frac{\varphi_1}{2i} \\ + \frac{(\varphi_2+\Delta\varphi_2)}{2i} G_0((\varphi_2+\Delta\varphi_2)(\varphi_2^*+\Delta\varphi_2^*)) + \frac{c}{2}(\varphi_2+\Delta\varphi_2) = 0 \end{array} \tag{54}$$

And,

$$\begin{array}{l} \frac{\partial(\varphi_2^*+\Delta\varphi_2^*)}{\partial\tau_0} + \frac{1}{2i}(\varphi_2^*+\Delta\varphi_2^*) - \frac{\varphi_1^*}{2i} \\ - \frac{(\varphi_2^*+\Delta\varphi_2^*)}{2i} G_0((\varphi_2+\Delta\varphi_2)(\varphi_2^*+\Delta\varphi_2^*)) + \frac{c}{2}(\varphi_2^*+\Delta\varphi_2^*) = 0 \end{array} \tag{55}$$

We perform the following Taylor development:

$$G_0((\varphi_2+\Delta\varphi_2)(\varphi_2^*+\Delta\varphi_2^*)) = G_0(\varphi_2\varphi_2^*) + (\varphi_2^*\Delta\varphi_2 + \varphi_2\Delta\varphi_2^*) G_0'(\varphi_2\varphi_2^*) + \mathcal{O}(|\Delta\varphi_2|^2) \tag{56}$$

These two equations Eqs. 54 and 55 can be simplified by neglecting the terms at the order $\mathcal{O}(|\Delta\varphi_2|^2)$. The equations can be expressed in matrix form, where components of the matrix $\mathbb{M}$ are defined in Appendix D.

$$\begin{bmatrix} \frac{\partial\Delta\varphi_2}{\partial\tau_0} \\ \\ \frac{\partial\Delta\varphi_2^*}{\partial\tau_0} \end{bmatrix} = \mathbb{M} \begin{bmatrix} \Delta\varphi_2 \\ \\ \Delta\varphi_2^* \end{bmatrix} \tag{57}$$

The reduced order system is stable if the real parts of the eigenvalues of $\mathbb{M}$ are negatives. The characteristic polynomial of the matrix $\mathbb{M}$ via $\det(\mathbb{M} - XI_2)$ reads as (I_2 is the 2×2 identity matrix):

$$X^2 + cX + P(N_2) \tag{58}$$

With,

$$\begin{array}{l} P(N_2) = -\frac{N_2^2}{2} G_0'(N_2^2) + N_2^2 \frac{G_0(N_2^2) G_0'(N_2^2)}{2} + \frac{G_0(N_2^2)^2}{4} \\ - \frac{G_0(N_2^2)}{2} + \frac{c^2}{4} + \frac{1}{4} \end{array} \tag{59}$$

The order of the characteristic polynomial is two. So, the sign of its roots can be determined. As $-c$ is always negative, then the sum of the two eigenvalues is negative. $P(N_2)$ is the product of the eigenvalues. Then, if $P(N_2)$ is negative, the two real parts of the eigenvalues are in opposite signs and one is positive so the fixed point is unstable. On the contrary, if $P(N_2)$ is positive, the two real parts of the eigenvalues have the same signs and they are negatives (as their sum is always negative) so the fixed point is stable.

3.3. Slow dynamics of the system

The multiple scale study started with the investigation on the fast time scale study in the previous section permitted us to obtain the SIM and its stability borders. Now, the slow time scale will be studied. The $\mathcal{O}(\epsilon^1)$ of the first equation of Eq. 39 reads:

$$\frac{\partial \varphi_1}{\partial \tau_1} = E_1(\varphi_1, \varphi_2, \varphi_1^*, \varphi_2^*) \tag{60}$$

With,

$$E_1 = \frac{\sigma}{2i}\varphi_1 - \frac{1}{2i}(\varphi_2 - \sigma\varphi_1) - \frac{\alpha-1}{2i}G_0(|\varphi_2|^2)\varphi_2 - \frac{C_p\varphi_1}{2} - \frac{c(\alpha-1)}{2}\varphi_2 + \Gamma_1 \tag{61}$$

The fast dynamics must be taken into account: let us study the evolution of the SIM at the time scale τ_1.

$$\begin{cases} \dfrac{\partial \mathscr{H}}{\partial \tau_1} = \dfrac{\partial \mathscr{H}}{\partial \varphi_1}\dfrac{\partial \varphi_1}{\partial \tau_1} + \dfrac{\partial \mathscr{H}}{\partial \varphi_2}\dfrac{\partial \varphi_2}{\partial \tau_1} + \dfrac{\partial \mathscr{H}}{\partial \varphi_1^*}\dfrac{\partial \varphi_1^*}{\partial \tau_1} + \dfrac{\partial \mathscr{H}}{\partial \varphi_2^*}\dfrac{\partial \varphi_2^*}{\partial \tau_1} = 0 \\ \dfrac{\partial \mathscr{H}^*}{\partial \tau_1} = \dfrac{\partial \mathscr{H}^*}{\partial \varphi_1}\dfrac{\partial \varphi_1}{\partial \tau_1} + \dfrac{\partial \mathscr{H}^*}{\partial \varphi_2}\dfrac{\partial \varphi_2}{\partial \tau_1} + \dfrac{\partial \mathscr{H}^*}{\partial \varphi_1^*}\dfrac{\partial \varphi_1^*}{\partial \tau_1} + \dfrac{\partial \mathscr{H}^*}{\partial \varphi_2^*}\dfrac{\partial \varphi_2^*}{\partial \tau_1} = 0 \end{cases} \tag{62}$$

This system can be expressed in the matrix form:

$$\underbrace{\begin{bmatrix} \dfrac{\partial \mathscr{H}}{\partial \varphi_2} & \dfrac{\partial \mathscr{H}}{\partial \varphi_2^*} \\ \dfrac{\partial \mathscr{H}^*}{\partial \varphi_2} & \dfrac{\partial \mathscr{H}^*}{\partial \varphi_2^*} \end{bmatrix}}_{B_2} \begin{bmatrix} \dfrac{\partial \varphi_2}{\partial \tau_1} \\ \dfrac{\partial \varphi_2^*}{\partial \tau_1} \end{bmatrix} = - \underbrace{\begin{bmatrix} \dfrac{\partial \mathscr{H}}{\partial \varphi_1} & \dfrac{\partial \mathscr{H}}{\partial \varphi_1^*} \\ \dfrac{\partial \mathscr{H}^*}{\partial \varphi_1} & \dfrac{\partial \mathscr{H}^*}{\partial \varphi_1^*} \end{bmatrix}}_{B_1} \begin{bmatrix} \dfrac{\partial \varphi_1}{\partial \tau_1} \\ \dfrac{\partial \varphi_1^*}{\partial \tau_1} \end{bmatrix} \tag{63}$$

Matrix B_1 and B_2 are detailed in Appendix E. According to this equation, two types of characteristic points can be defined:

Equilibrium point:
$$\begin{cases} E_1 = 0 \\ \mathscr{H} = 0 \\ \det(B_2) \neq 0 \end{cases}$$

Singular point:
$$\begin{cases} E_1 = 0 \\ \mathscr{H} = 0 \\ \det(B_2) = 0 \end{cases}$$

It can be seen that $B_2 = -\mathbb{M}$ where $\mathbb{M}$ is the matrix defined in Eq. 57. So, the matrix B_2 has the same characteristic equation which is defined in Eq. 58, i.e. $\det(B_2) = P(N_2)$. Hence, the amplitudes of singular points are situated on the boundary of the unstable zone of the SIM. To find the equilibrium points, the equation $E_1 = 0$ has to be solved, in terms of amplitude N_2 including the fast dynamics ($\mathscr{H} = 0$). Fast and slow dynamics are clarified for the system coupled with a NES with general excitation. In the following sections, the results will be detailed for the two types of excitation.

3.4. Dynamics of the system without the NES under the aerodynamic excitation

In this section, the multiple scale method described in the previous section will be used to detect the dynamical behavior of the system without the NES under aerodynamic excitation. The general dynamic equation of this case can be deducted from Eqs. 19 and 32 by eliminating terms related to the NES:

$$\ddot{p}_k(\tau) + \epsilon C_p \dot{p}_k + p_k(\tau) = \epsilon \left(\alpha_0 - \alpha_1 \dot{p}_k - \alpha_2 \dot{p}_k^2 - \alpha_3 \dot{p}_k^3\right) \tag{64}$$

The complex variable φ_1 is introduced:

$$\varphi_1 e^{i\Omega\tau} = \dot{p}_k + i\Omega p_k \tag{65}$$

Where i is the imaginary number with $i^2 = -1$ and Ω is the angular frequency of the system. The detuning parameter σ is introduced as: $\Omega = 1 + \epsilon\sigma$. The Eq. 64 is rewritten with the complex variable and only the first harmonic is retained involving the following equation:

$$\frac{\partial \varphi_1}{\partial \tau} - \frac{\Omega \varphi_1}{2i} + \epsilon \frac{C_p \varphi_1}{2} + \frac{\varphi_1}{2i\Omega} = -\epsilon \frac{\alpha_1 \varphi_1}{2} - \epsilon \frac{3\alpha_3 \varphi_1^2 \varphi_1^*}{8} \tag{66}$$

$\mathcal{O}(\epsilon^0)$ of Eq. 66 becomes:

$$\frac{\partial \varphi_1}{\partial \tau_0} - \frac{\varphi_1}{2i} + \frac{\varphi_1}{2i} = 0 \Rightarrow \frac{\partial \varphi_1}{\partial \tau_0} = 0 \tag{67}$$

Then, $\mathcal{O}(\epsilon^1)$ of Eq. 66 reads:

$$\frac{\partial \varphi_1}{\partial \tau_1} - \frac{\sigma}{2i}\varphi_1 + \frac{C_p}{2}\varphi_1 - \frac{\sigma}{2i}\varphi_1 = \frac{\alpha_1}{2}\varphi_1 - \frac{3\alpha_3}{8}\varphi_1^2 \varphi_1^* \tag{68}$$

The equilibrium points of this system can be found by setting $\dfrac{\partial \varphi_1}{\partial \tau_1} = 0$. Considering $\varphi_1 = N_1 e^{i\delta_1}$, $N_1 \in \mathbb{R}^+$, $\delta_1 \in \mathbb{R}$, we will have:

$$N_1 \left(\frac{C_p}{2} - \frac{\sigma}{i} + \frac{\alpha_1}{2}\right) = -\frac{3\alpha_3}{8} N_1^3 \tag{69}$$

This complex equation provides $\sigma = 0$. Then, the equation has a trivial solution $N_1 = 0$. The non-trivial solutions of the system are defined as:

$$N_1^2 = -\frac{8}{3\alpha_3}\left(\frac{C_p}{2} + \frac{\alpha_1}{2}\right) \tag{70}$$

This equation can be easily solved if the following condition is respected:

$$-\frac{8}{3\alpha_3}\left(\frac{C_p}{2} + \frac{\alpha_1}{2}\right) > 0 \tag{71}$$

We can distinguish all cases concerning the sign of α_1 and α_3 but we concentrate on one case. That is the case mentioned in the paper of Chabart [41] when the

initial angle of attack of the wind is -165° where $\alpha_1 < 0$ and $\alpha_3 > 0$. In this case, The condition from the Eq. 71 will be respected if the wind speed is higher that a certain value called the critical wind speed U_c. The critical wind speed is expressed as:

$$U_c = -\frac{2\epsilon m \omega_k C_p}{\rho_f b A_1} \tag{72}$$

So, when the wind speed is lower than the critical wind speed, the only equilibrium point is $N_1 = 0$ and when the wind speed is higher, there are two equilibrium points, one is $N_1 = 0$ and the second can be expressed as:

$$N_1 = \sqrt{-\frac{8}{3\alpha_3}\left(\frac{C_p}{2} + \frac{\alpha_1}{2}\right)} \tag{73}$$

A stability analysis of these equilibrium points reveals that before the critical wind speed, the solution is stable and after the critical wind speed, the solution $N_1 = 0$ is unstable but the other solution is stable. In other words, we have here a super-critical Hopf bifurcation.

3.5. The slow dynamics of the system coupled to a NES with the two considered excitations

In this section, developed techniques for the detection of slow dynamics of a coupled system described in section 3, will be used for the system under two different types of excitation namely, harmonic and aerodynamic excitation.

3.5.1. The system under harmonic excitation

Setting $\Omega = 1 + \sigma\epsilon$ in Eq. 23 and keeping its first harmonic, we will have:

$$\Gamma_1 = \frac{\gamma}{2i} \tag{74}$$

Then Eq. 62 which provides equilibrium points of the system yields to:

$$\begin{aligned} &N_2^2\left(\frac{G_0(|\varphi_2|^2)(2\sigma + (\alpha - 1))}{2} - \sigma + \frac{C_p c}{2} + \frac{1}{2}\right)^2 \\ &+N_2^2\left(\frac{C_p G_0(|\varphi_2|^2)}{2} - \sigma c - \frac{C_p + c(\alpha - 1)}{2}\right)^2 = \frac{\gamma^2}{4} \end{aligned} \tag{75}$$

Eq. 75 can be solved numerically. The simplest way is to organize this equation as a second order polynomial with respect to σ, so a certain range of N_2 values can be considered and different σ value can be obtained for each N_2 value. Then, with the SIM for each N_2 value, the corresponding N_1 value can be calculated. The reorganized equation reads:

$$\Lambda_1\sigma^2 + \Lambda_2\sigma + \Lambda_3 = 0 \tag{76}$$

With,

$$\begin{aligned}
\Lambda_1 = &\quad N_2^2(1-G_0)^2 + N_2^2 c^2 \\
\Lambda_2 = &\quad -2N_2^2(1-G_0)\left(\frac{C_p c}{2} + \frac{1}{2} + \frac{\alpha-1}{2}G_0\right) \\
&\quad +2N_2^2 c\left(\frac{C_p c}{2}(1-G_0) + \frac{c(\alpha-1)}{2}\right) \\
\Lambda_3 = &\quad N_2^2\left(\frac{C_p c}{2} + \frac{1}{2} + \frac{\alpha-1}{2}G_0\right)^2 \\
&\quad +N_2^2\left(\frac{C_p c}{2}(1-G_0) + \frac{c(\alpha-1)}{2}\right)^2 - \frac{\gamma^2}{4}
\end{aligned} \tag{77}$$

3.5.2. The system under aerodynamic excitation

The non-dimensional expression of the aerodynamic force was given in the section 2 (see Eq. 32), reads:

$$\epsilon\Gamma = \epsilon\left(\alpha_0 - \alpha_1(\dot{w} + \epsilon\dot{v}) - \alpha_2(\dot{w} + \epsilon\dot{v})^2 - \alpha_3(\dot{w} + \epsilon\dot{v})^3\right) \tag{78}$$

The first harmonic of this function becomes:

$$\Gamma_1 = \frac{\Omega}{2\pi}\int_0^{\frac{2\pi}{\Omega}} \Gamma e^{-i\Omega\tau}\mathrm{d}\tau = -\alpha_1\frac{\varphi_1}{2} - \alpha_3\frac{3\varphi_1^2\varphi_1^*}{8} + \mathcal{O}(\epsilon) \tag{79}$$

After introducing Γ_1 in the equation $E_1 = 0$, and taking account of the relation between φ_1 and φ_2 (Eq. 51), a complex equation which can be factorized by φ_2 is obtained. Hence, $\varphi_2 = 0$ is always a solution of this system. As we are looking for non zero solutions, the equation $E_1 = 0$ can be divided by φ_2 and separated in two real equations:

$$\begin{cases}
\sigma = \dfrac{1-\alpha}{2} - \dfrac{1}{c}\left(1 - G_0(|\varphi_2|^2)\right)h(N_2) \\[2ex]
h(N_2)\left(c + \dfrac{1}{c}\left(1 - G_0(|\varphi_2|^2)\right)^2\right) + \dfrac{\alpha}{2} = 0
\end{cases} \tag{80}$$

With,

$$h(N_2) = \frac{C_p}{2} + \frac{\alpha_1}{2} + \frac{3\alpha_3}{8}\varphi_2\varphi_2^*\left(\left(1 - G_0(|\varphi_2|^2)\right)^2 + c^2\right) \tag{81}$$

This equation is nonlinear, the three main variables are N_2, σ and U the energy of the NES, the detuning parameter ans the wind speed. The wind speed U is hidden in α_3 and α_1, so we set:

$$\begin{aligned}
\alpha_1 &= U\tilde{\alpha}_1 \\
\alpha_3 &= \frac{\tilde{\alpha}_3}{U}
\end{aligned} \tag{82}$$

Where $\tilde{\alpha}_1$ and $\tilde{\alpha}_3$ do not depend on U. It is seen that Eq. 80 is a second order polynomial with respect to U. The second equation of Eq. 80 can be rewritten as:

$$\xi_1 U^2 + \xi_2 U + \xi_3 = 0 \tag{83}$$

With,

$$\xi_1 = \frac{\tilde{\alpha}_1}{2}$$

$$\xi_2 = \frac{C_p}{2} + \frac{\alpha}{2\left(c + \frac{1}{c}(1-G_0)^2\right)} \tag{84}$$

$$\xi_3 = \frac{3\tilde{\alpha}_3}{8} N_2^2 \left((1-G_0)^2 + c^2\right)$$

So, for a range of N_2 values the solutions of Eq. 83 can be found for each N_2 values. This procedure leads to bifurcation diagrams of the overall system. In addition of the calculated equilibrium points the trivial solutions $(N_2, N_1) = (0, 0)$ remains. We will assume that those solutions are stable if there are no other solutions and unstable if we can find non zero equilibrium points.

4. Finite element modelling of the system and validation of the analytical predictions

In the last sections, the analytical results have been presented for the detection of different dynamics of a beam with elastic boundary conditions coupled to non-smooth NES. In this part, a finite element model of the system is presented and obtained numerical results are compared with those obtained from analytical predictions. The finite element software (Code_Aster) that we are using does not permit to model aerodynamic excitation. For this reason, this section will be only on the harmonic excitation.

4.1. The finite element model of the system

The beam with elastic boundary conditions coupled to a NES that is described in Fig. 1 is modeled with a finite element method using the software Code_Aster. One-dimensional linear beam elements are used for modeling the primary system and the boundary conditions are modeled by discrete elements that behave as linear rotational and translational springs. The non-smooth NES is designed with a material which changes its rigidity after a clearance of 2δ from K_1 to K_2, hence the behavior of the NES is the same as the one described in Fig. 4 with $K_1 = 0$ and $K_2 = K$.
Table 1 provides the physical characteristics of the beam and its boundary conditions. The mode shapes are calculated by the analytic method described in section 2 and also by a modal analysis via the finite element method. Fig. 5 shows that the results of both methods are in good agreement.

In this study, the behavior of the system is examined around the first mode whose frequency is 0.407 Hz. The NES is attached to the middle of the beam, so $l_n = 2\ m$. The analytical equations are projected on the first mode of the beam and the excitation frequency is close to the frequency of the first mode. The parameters of the NES used for analytical developments are presented in

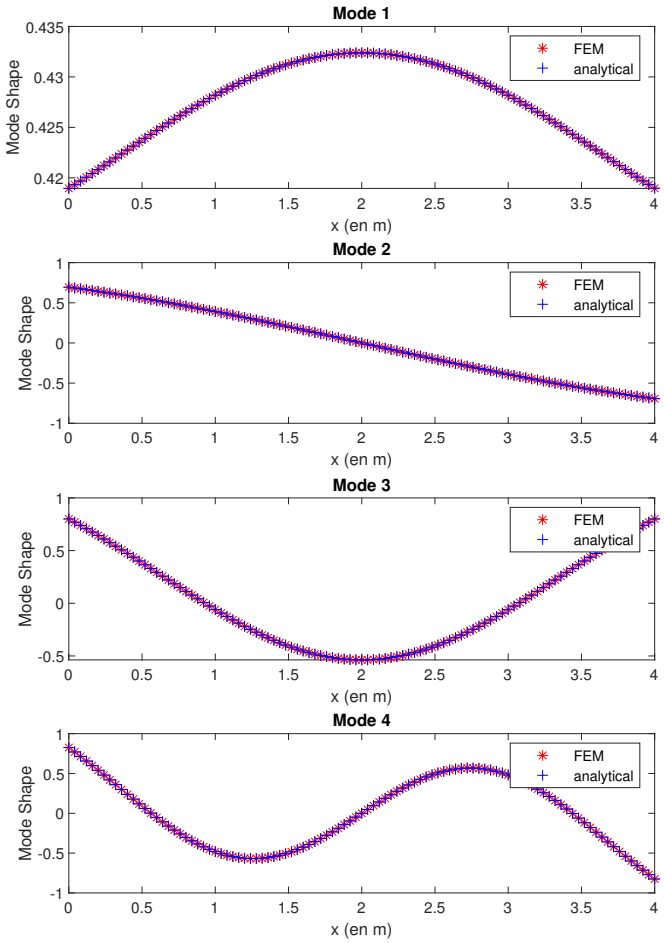

Figure 5: The mode shape of the linear beam with elastic boundary conditions determined by the finite element method (FEM) and the analytical method.

$k_0\ (N.m^{-1})$	$k_L\ (N.m^{-1})$	$k_{R0}\ (N.m.rad^{-1})$	$k_{RL}\ (N.m.rad^{-1})$
18.27	18.27	286.6	286.6
$L\ (m)$	$E\ (GPa)$	$I\ (m^4)$	$m\ (Kg.m^{-1})$
4	68.3	8.3923×10^{-9}	1.369

Table 1: Physical characteristics of the linear beam and its boundary conditions.

Table 2,while the correspondences of the same parameters in physical domain are summarized in Table 3. The excitation F_1 and F_2 reads as:

$$F_1(t) = F_2(t) = F\sin(\Omega_r t) \tag{85}$$

With F the amplitude of the force and Ω_r the angular frequency of the external excitations.

k_1	k_2	c	$\bar{\delta}$	ϵ	C_p	γ
0	1.5	0.25	0.2	0.001	20	5

Table 2: Analytical parameters for the study of the non-smooth NES and the system.

c_{NES}	K_1	K_2
$3.502 \times 10^{-3}\ N.m^{-1}.s$	$0\ N.m^{-1}$	$5.374 \times 10^{-2}\ N.m^{-1}$
δ	m_{NES}	F
$0.8\ m$	$5.476 \times 10^{-3}\ Kg$	$0.3611\ N$

Table 3: Physical characteristics of the non-smooth NES.

Finally, the damping of the primary system is provided by a function of Code_Aster that enables to add modal damping. In the analytic model, damping of the primary system is defined by a viscous term C. Let us suppose that ξ is the coefficient of Rayleigh damping of the primary system:

$$\xi = \frac{C}{2m\omega_k} \tag{86}$$

The analytical damping parameter of the primary system is $C_p = 20$ which correspond to $\xi = 1\%$. So, a model damping of 1% is provided on the studied mode by the function of Code_Aster. In the next subsection, obtained results for the system coupled to chosen non-smooth NES will be presented.

4.2. The system with coupled non-smooth NES under harmonic excitation

In this section, the results obtained with the non-smooth NES are presented. All the analytical parameters of the system have been defined in Table 2. They correspond to the physical parameters in Table 3.
First, we have the results for the free vibration system obtained by the numerical integration of Eqs. 35 and 36 by a Runge-Kutta method (ODE45 in

$c_{NES}\ (N.m^{-1})$	$k_{NES}\ (N.m^{-1})$	$m_{NES}\ (Kg)$	$F\ (N)$
3.502×10^{-3}	5.598×10^{-4}	5.476×10^{-3}	1.625

Table 4: Physical characteristics of the cubic NES.

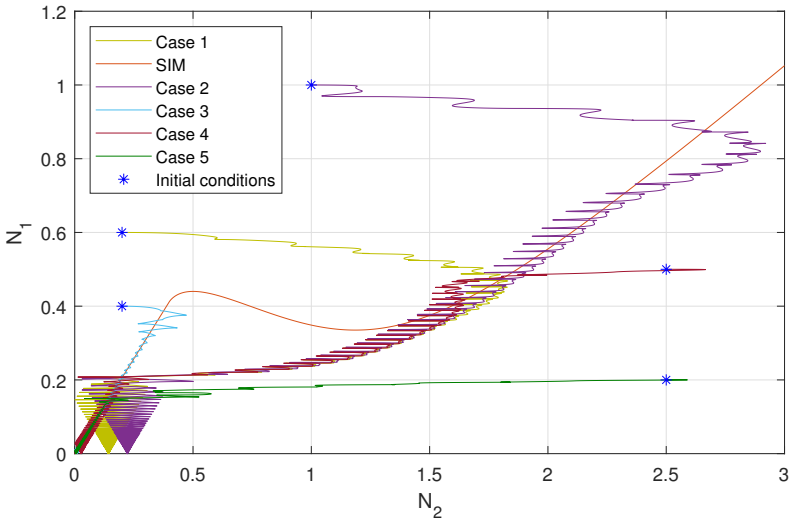

Figure 6: Numerical simulation by numerical integration of the free vibration system (nonsmooth NES) for different initial boundary conditions.

Matlab). In Fig. 6, the evolution of N_1 versus N_2 is plotted for different initial conditions. The trajectory follows the stable branch of the SIM and bifurcates at the stability border to the other stable branch. We can see that the different trajectories end at different points, this is because gravity is not taken into account and $k_1 = 0$ so there is an infinity of static equilibrium position. For the beam, only $v = 0$ is the solution for the static, but for the NES, if $k_1 = 0$ all the values in the interval $[-\delta, \delta]$ are the solution for u of the static problem.
The equilibrium points for the system under the harmonic excitation are investigated. Fig. 7 and 8 shows the equilibrium points of the system obtained from analytical predictions and the equilibrium state obtained for different frequency via numerical methods. The numerical results fit well with the analytical predictions.

5. Control of aerodynamic instability with a non smooth NES

The purpose of this section is to study the control potential of the piecewise linear NES on aerodynamic instability of a cable. Chabart et al. [41] generated experimentally an aerodynamic instability on a portion of a cable with ice-accretion. The outside layer of a conductor is installed on a 0.8 meters long

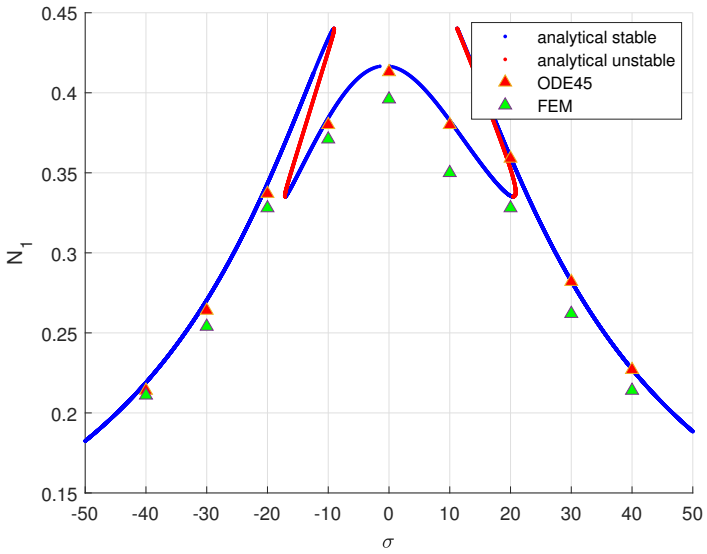

Figure 7: Comparison of the equilibrium points of the system with the non-smooth NES for sweeping frequency obtained from analytical, the finite element, and the numerical integrations.

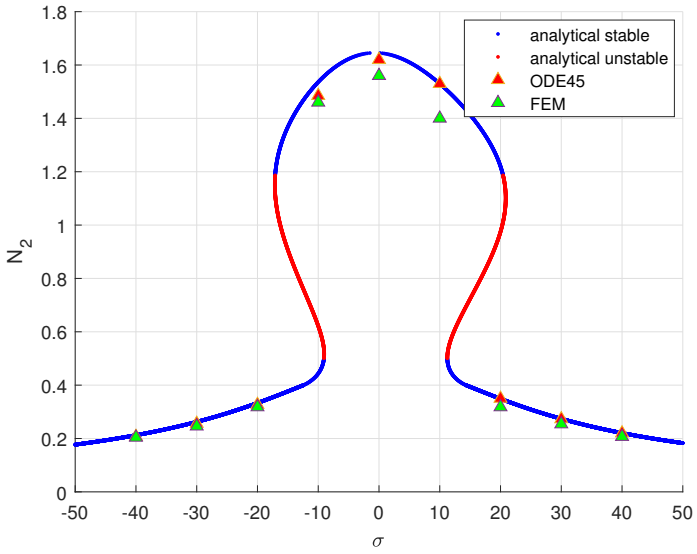

Figure 8: Comparison of the equilibrium points of the system with the non-smooth NES for sweeping frequency obtained from analytical, the finite element and the numerical integrations.

rigid tube, and an artificial ice cross-section is added. First, an aerodynamic test was performed to provide the aerodynamic coefficients given on the Fig. 3. Then, the cable portion was suspended by springs and placed on the wind tunnel to perform aeroelastic tests at different angles of attack. For the aeroelastic test, the natural frequency of the vertical motion is 0.845 Hz, the total mass of the device is 2.99 Kg, and the damping of the system is about 0.08%. The experimental device was placed in a wind tunnel. In this section, our model will be adapted to be similar to the aeroelastic test which was performed by Chabart [41]. The test that we are interested on is the one with an inital angle of attack of $-165°$, as it shows a vertical galloping behavior. As our model only takes into account vertical motion, this study is focused on this case. The Table 5 shows the parameters of the linear beam with elastic boundary conditions. Compared to the configuration of the previous section, the length of the beam,

k_0 $(N.m^{-1})$	k_L $(N.m^{-1})$	k_{R0} $(N.m.rad^{-1})$	k_{RL} $(N.m.rad^{-1})$
42.14	42.14	0	0
L (m)	E (GPa)	I (m^4)	m $(Kg.m^{-1})$
0.8	68.3	8.3923×10^{-9}	3.7375

Table 5: Physical characteristics of the linear beam and its boundary conditions for the aeroelastic test.

the linear mass, and the translational springs have been adjusted in order to have the same natural frequency and the same mass as the experimental test. The damping coefficient of the system is set to $0,08\%$. The coefficient of the aerodynamic force defined in the Eq. 30 can be calculated by interpolation of the aerodynamic function (Fig. 3) concerning α around the angle of attack $\alpha = 165°$ (which corresponds to the angle of attack $-165°$ in the paper). The coefficients are given as:

$$\begin{aligned} A_0 &= 0.131 \\ A_1 &= -0.9233 \\ A_2 &= 2.8354 \\ A_3 &= 1.4718 \end{aligned} \tag{87}$$

The analytical results from section 3.4 allow to determine the bifurcation diagram of this system without a NES. The physical properties needed in the analytic procedure are listed in the Table 6. The analytical parameters defined

ω_k $(rad.s^{-1})$	ρ_f $(Kg.m^{-3})$	b (m)
5.31	1.184	32.5×10^{-3}

Table 6: Physical properties of the system for the aeroelastic configuration.

in section 2 are shown in Table 7. The parameters ϵ and l_n are related to the NES, they are arbitrary chosen when there is no NES. Here, they will be the same as the configuration with the NES.

α_0/U^2 $(m^{-2}.s^2)$	α_1/U $(m^{-1}.s)$	α_2	$\alpha_3.U$ $(m.s^{-1})$
0.0539	-0.1119	1.1677	2.5745
ϵ	C_p	l_n/L	
0.01	0.16	0.5	

Table 7: Necessary parameters of the system under aerodynamic excitation (for analytical predictions).

The bifurcation diagram of the system is shown on the Fig. 9. The equilibrium points of the system obtained by numerical integration of Eq. 64 are also shown on the same figure. The two zones separated by the critical wind speed $U_c = 1.4298 \ \ m.s^{-1}$ can be clearly distinguished. The first zone only has one stable branch where $N_1 = 0$. The second zone also called the post-critical zone, contains two branches, one is unstable with $N1 = 0$ and the other is non zero. As the initial condition for the numerical integration is non zero, the system is systematically attracted by the stables solutions.

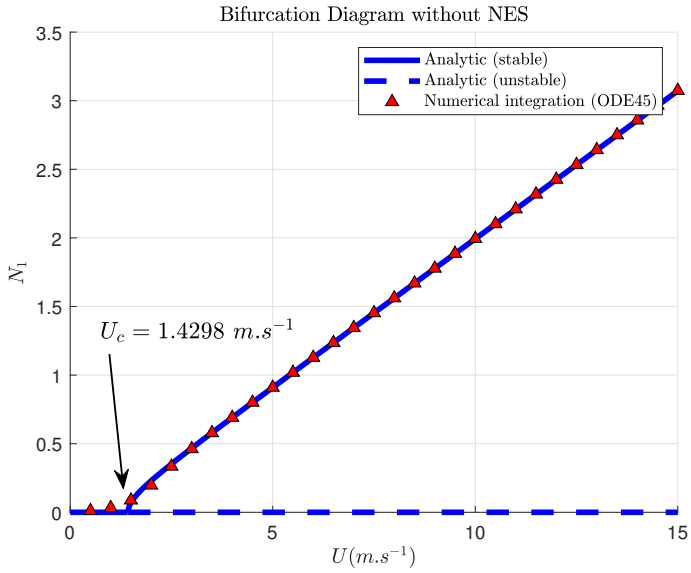

Figure 9: Bifurcation diagram of the system without NES obtained with the analytic method and equilibrium points obtained by numerical integration.

The same study is carried out for the system with a coupled NES. The parameters of the chosen NES are shown on the Table 8. The bifurcation diagrams for the system with (the same as Fig. 9) and without the NES are shown on the Fig. 10. The equilibrium points of the system with the NES are obtained by the analytic procedure described in the section 3.5. Two types of equilibrium points are shown, in blue they are coming from the stable zones of the SIM, and in red which correspond to these coming from the unstable zone of the SIM. We can see

ϵ	l_n/L	k	c	δ
0.01	0.5	2	0.3	0.3

Table 8: Analytical parameters of the NES for the aeroelastic configuration.

that for a given wind speed, several equilibrium points can exist. The Fig. 10 also shows the equilibrium points provided by the numerical integration of the Eqs. 35 and 36. The numerical integration of the system with the NES shows that the system is attracted by the non-zero solution when there is one zero solution and one non-zero solution. When there are several non-zero solutions, the system is attracted by the solution coming from the unstable zone of the SIM. To obtain the equilibrium points of the system by numerical integration, an averaging of the last periods of the signal has been carried out. So when the system is attracted by the equilibrium points coming from the unstable zone of the SIM, it will present strong modulated response (SMR) and presented results in Fig. 10, correspond to the average of SMR during a given time interval. Let us consider a case with $U = 10\ m.s^{-1}$ which is presented in Fig. 11. It is seen that the SMR oscillates between the two stable branches of the SIM by a recurrence of bifurcations from one stable branch to the other.

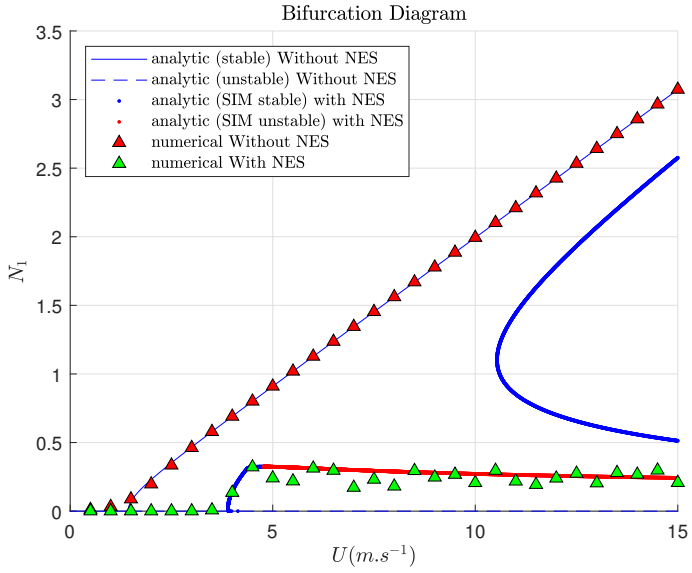

Figure 10: Bifurcation diagram of the system with and without the NES obtained with the analytic method and equilibrium points obtained by numerical integration.

If we look a the temporal response of the system with and without the NES of a wind speed of $U = 10\ m.s^{-1}$ (Fig. 12), we can see the significant reduction of the amplitude of the primary system due to the non smooth NES. This section shows the results system behavior under aerodynamic instability

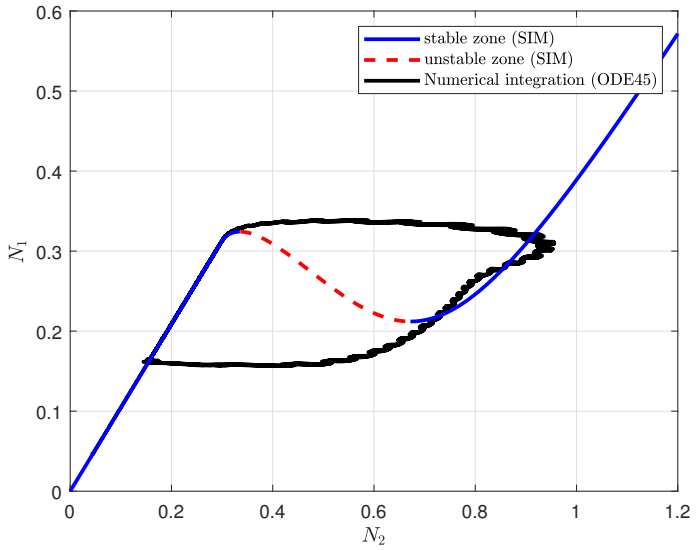

Figure 11: Response of the system with NES when $U = 10\ m.s^{-1}$ obtained by numerical integration (black curve) in the 2D-plan N_1 vs. N_2, with the SIM (stable zones in blue and unstable zone in red).

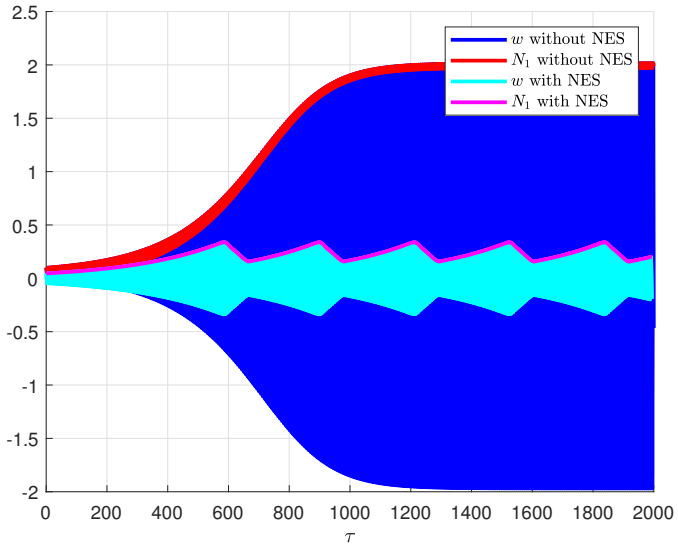

Figure 12: Time history response of the system with (magenta and cyan curves) and without (red and blue curves) NES when $U = 10\ m.s^{-1}$ obtained by numerical integration.

and the impact of the NES in terms of galloping mitigation. We have to point out that some assumptions have been made here which make the system a bit far from the reality. The gravity is neglected and the real nonlinear behaviors of a suspended cable are not taken into account [34], [44]. However, some major characteristics of the galloping oscillations of a cable are well modeled here as the really soft behavior of the system, the self excited behavior and the large oscillations amplitude. Even if the NES is not optimized here, the results show a great potential for galloping mitigation.

6. Conclusion

The passive control of a linear beam element with elastic boundary conditions by a nonlinear energy sink with piecewise linear nonlinearity is studied. First the system is studied under harmonic excitation. As the goal is to study galloping oscillations on overhead transmission lines, the system is also studied under aerodynamic excitation. After the projection of the overall system on an arbitrary mode of interest, a complexed form of the coupled governing equations are treated by multiple scale method. Then, different system dynamics are detected leading to the tracing of slow invariant manifold and equilibrium singular points of the system. Obtained frequency response curves allow having predictions on possible system behaviors for given driving frequency and forcing amplitude. All analytical predictions are confronted by numerical results obtained by direct numerical integration of system equations and also those which are obtained by finite element modeling of overall structure showing a good agreement between all results. Experimental data from literature are used to implement an aerodynamic excitation which leads to an aerodynamic instability. Bifurcation diagram are obtained for the system with and without the nonlinear energy sink. The post-critical behavior of the system with the nonlinear energy sink present periodic and quasi-periodic solutions. Results shows the great potential of the piecewise linear nonlinear energy sink to mitigate galloping oscillations. This work provides a complete analytical tools to investigate the impact of a nonlinear energy sink on continuous structure as a cable or a beam. Finally, this study gives prospects to study galloping control of a transmission line conductor with a piecewise linear nonlinear energy sink. The non linear behavior of the suspended cable can be taken into account by implementing a nonlinear cable model with zero bending stiffness, only axial stress in traction, and with geometrical nonlinearities induced by the static deformed shape which is the consequence of gravity on the cable.

Acknowledgments

The authors would like to thank the "Institut Carnot, Ingénérie@Lyon" for partially supporting this research in the framework of the "CONOG" project.

Appendix A. Mode Shape of primary system

The terms of the matrix $M = (m_{ij})_{i,j\in[1..4]^2}$ from Eq. 8 can be calculated, the boundary conditions from Eq. 2 and Eq. 3 with the form of F and Φ from Eq. 6 and Eq. 7. To simplify the expressions the following non-dimensional parameters are introduced :

$$\bar{k}_0 = \frac{k_0 L^3}{EI} \; ; \; \bar{k}_L = \frac{k_L L^3}{EI} \; ; \; \bar{k}_{R0} = \frac{k_{R0} L}{EI} \; ; \; \bar{k}_{RL} = \frac{k_{RL} L}{EI} \; ; \; \bar{\beta} = \beta L \tag{A.1}$$

$$\begin{aligned}
m_{14} &= -m_{11} = \bar{\beta}^3 \\
m_{12} &= m_{13} = \bar{k}_0 \\
m_{21} &= m_{24} = \bar{k}_{R0} \\
m_{22} &= -m_{23} = \bar{\beta} \\
m_{31} &= -\bar{\beta}^3 \cos\bar{\beta} - \bar{k}_L \sin\bar{\beta} \\
m_{32} &= \bar{\beta}^3 \sin\bar{\beta} - \bar{k}_L \cos\bar{\beta} \\
m_{33} &= \bar{\beta}^3 \sinh\bar{\beta} - \bar{k}_L \cosh\bar{\beta} \\
m_{34} &= \bar{\beta}^3 \cosh\bar{\beta} - \bar{k}_L \sinh\bar{\beta} \\
m_{41} &= -\bar{\beta} \sin\bar{\beta} + \bar{k}_{RL} \cos\bar{\beta} \\
m_{42} &= -\bar{\beta} \cos\bar{\beta} - \bar{k}_{RL} \sin\bar{\beta} \\
m_{43} &= \bar{\beta} \cosh\bar{\beta} + \bar{k}_{RL} \sinh\bar{\beta} \\
m_{44} &= \bar{\beta} \sinh\bar{\beta} + \bar{k}_{RL} \cosh\bar{\beta}
\end{aligned} \tag{A.2}$$

The solutions β_i of the equation $\det(M) = 0$ gives the natural frequencies ω_i. Then, by inverting the system of Eq. 8 the expression of the modes shapes are given depending on a constant α.

$$\Phi_i(x) = \alpha \left(V_1 \sin(\beta_i x) + V_2 \cos(\beta_i x) + V_3 \cosh(\beta_i x) + V_4 \sinh(\beta_i x) \right) \tag{A.3}$$

$$V = \begin{bmatrix} V_1 \\ V_2 \\ V_3 \\ V_4 \end{bmatrix} = \begin{bmatrix} \left(K \dfrac{\bar{\beta}_i^4 - \bar{k}_{R0}\bar{k}_0}{\bar{k}_{R0}\bar{k}_0 + \bar{\beta}_i^4} - \dfrac{2\bar{k}_{R0}\bar{\beta}_i^3}{\bar{k}_{R0}\bar{k}_0 + \bar{\beta}_i^4} \right) \dfrac{\bar{k}_0}{\bar{\beta}_i^3} + K \dfrac{\bar{k}_0}{\bar{\beta}_i^3} + 1 \\ K \dfrac{\bar{\beta}_i^4 - \bar{k}_{R0}\bar{k}_0}{\bar{k}_{R0}\bar{k}_0 + \bar{\beta}_i^4} - \dfrac{2\bar{k}_{R0}\bar{\beta}_i^3}{\bar{k}_{R0}\bar{k}_0 + \bar{\beta}_i^4} \\ K \\ 1 \end{bmatrix} \tag{A.4}$$

$$K = \frac{\dfrac{2\bar{k}_{R0}\bar{\beta}_i^3}{\bar{k}_{R0}\bar{k}_0 + \bar{\beta}_i^4} - \dfrac{\bar{\beta}_i^3\left(\bar{\beta}_i \sinh\bar{\beta}_i + \bar{k}_{RL}\cosh\bar{\beta}_i\right) + \bar{\beta}_i^3\left(-\bar{\beta}_i \sin\bar{\beta}_i + \bar{k}_{RL}\cos\bar{\beta}_i\right)}{-\bar{\beta}_i^3\left(\bar{\beta}_i \cos\bar{\beta}_i + \bar{k}_{RL}\sin\bar{\beta}_i\right) + \bar{k}_0\left(-\bar{\beta}_i \sin\bar{\beta}_i + \bar{k}_{RL}\cos\bar{\beta}_i\right)}}{\dfrac{\bar{\beta}_i^3\left(\bar{\beta}_i \cosh\bar{\beta}_i + \bar{k}_{RL}\sinh\bar{\beta}_i\right) + \bar{k}_0\left(-\bar{\beta}_i \sin\bar{\beta}_i + \bar{k}_{RL}\cos\bar{\beta}_i\right)}{-\bar{\beta}_i^3\left(\bar{\beta}_i \cos\bar{\beta}_i + \bar{k}_{RL}\sin\bar{\beta}_i\right) + \bar{k}_0\left(-\bar{\beta}_i \sin\bar{\beta}_i + \bar{k}_{RL}\cos\bar{\beta}_i\right)} - \dfrac{\bar{k}_{R0}\bar{k}_0 - \bar{\beta}_i^4}{\bar{k}_{R0}\bar{k}_0 + \bar{\beta}_i^4}} \tag{A.5}$$

The constant α can be determined when the mode shapes are normalized by the mass.

$$\alpha = \sqrt[-1]{mA} \tag{A.6}$$

$$\begin{aligned}
A &= \int_0^L \left(V_1 \sin(\beta_i x) + V_2 \cos(\beta_i x) + V_3 \cosh(\beta_i x) + V_4 \sinh(\beta_i x)\right)^2 dx \\
&= V_1^2 \left(\frac{L}{2} - \frac{\sin(2\beta_i L)}{4\beta_i}\right) + V_1 V_3 \left(\frac{\sin(\beta_i L)\sinh(\beta_i L) - \cos(\beta_i L)\cosh(\beta_i L) + 1}{\beta_i}\right) \\
&+ V_2^2 \left(\frac{L}{2} + \frac{\sin(2\beta_i L)}{4\beta_i}\right) + V_1 V_4 \left(\frac{\sin(\beta_i L)\cosh(\beta_i L) - \cos(\beta_i L)\sinh(\beta_i L)}{\beta_i}\right) \\
&+ V_3^2 \left(\frac{\sinh(2\beta_i L)}{4\beta_i} + \frac{L}{2}\right) + V_2 V_3 \left(\frac{\cos(\beta_i L)\sinh(\beta_i L) + \sin(\beta_i L)\cosh(\beta_i L)}{\beta_i}\right) \\
&+ V_4^2 \left(\frac{\sinh(2\beta_i L)}{4\beta_i} - \frac{L}{2}\right) + V_2 V_4 \left(\frac{\sin(\beta_i L)\sinh(\beta_i L) + \cos(\beta_i L)\cosh(\beta_i L) - 1}{\beta_i}\right) \\
&+ V_1 V_2 \left(\frac{1 - \cos^2(\beta_i L)}{\beta_i}\right) + V_3 V_4 \left(\frac{\cosh^2(\beta_i L) - 1}{\beta_i}\right)
\end{aligned}$$

Appendix B. Orthogonality of mode shapes

In this appendix the proof of orthogonality of modes for considered general boundary conditions is given: $\int_0^L \Phi_i \Phi_j dx = 0$ for $i \neq j$. Eq. 5 rewrites as:

$$\frac{d^4\Phi_i}{dx^4} = \beta_i^4 \Phi_i \Rightarrow \int_0^L \frac{d^4\Phi_i}{dx^4}\Phi_j dx = \beta_i^4 \int_0^L \Phi_i \Phi_j dx$$

By two integrations by parts we show that $\int_0^L \frac{d^4\Phi_i}{dx^4}\Phi_j dx$ is symmetric by the index i et j. We use the boundary conditions shown in Eqs. 2 and 3.

$$\begin{aligned}
\int_0^L \frac{d^4\Phi_i}{dx^4}\Phi_j dx &= \left[\Phi_j \frac{d^3\Phi_i}{dx^3}\right]_0^L - \left[\frac{d\Phi_j}{dx}\frac{d^2\Phi_i}{dx^2}\right]_0^L + \int_L^0 \frac{d^2\Phi_i}{dx^2}\frac{d^2\Phi_j}{dx^2}dx \\
&= \Phi_j(L)\frac{d^3\Phi_i}{dx^3}(L) - \Phi_j(0)\frac{d^3\Phi_i}{dx^3}(0) - \frac{d\Phi_j}{dx}(L)\frac{d^2\Phi_i}{dx^2}(L) \\
&+ \frac{d\Phi_j}{dx}(0)\frac{d^2\Phi_i}{dx^2}(0) + \int_L^0 \frac{d^2\Phi_i}{dx^2}\frac{d^2\Phi_j}{dx^2}dx \\
&= -\frac{k_L}{EI}\Phi_j(L)\Phi_i(L) + \frac{k_0}{EI}\Phi_j(0)\Phi_i(0) + \frac{k_{RL}}{EI}\frac{d\Phi_j}{dx}(L)\frac{d\Phi_i}{dx}(L) \\
&- \frac{k_{R0}}{EI}\frac{d\Phi_j}{dx}(0)\frac{d\Phi_i}{dx}(0) + \int_L^0 \frac{d^2\Phi_i}{dx^2}\frac{d^2\Phi_j}{dx^2}dx
\end{aligned} \tag{B.1}$$

The last expression of Eq. B.1 is symmetric by the index i et j. So we can write:

$$\begin{aligned}
&\int_0^L \frac{d^4\Phi_i}{dx^4}\Phi_j dx - \int_0^L \frac{d^4\Phi_j}{dx^4}\Phi_i dx = (\beta_i^4 - \beta_j^4)\int_0^L \Phi_i\Phi_j dx \\
\Leftrightarrow\ & 0 = (\beta_i^4 - \beta_j^4)\int_0^L \Phi_i\Phi_j dx \\
\Leftrightarrow\ & \int_0^L \Phi_i\Phi_j dx = 0 \ \text{ as } \ \beta_i \neq \beta_j
\end{aligned}$$

The modes shapes are orthogonal.

Appendix C. Non-dimentionalized parameters

$$\begin{aligned}
&\bar{u}(\tau) = \frac{u(t)}{L} \ \ ; \ \ \bar{\Phi}_k(\bar{x}) = \Phi_k(x) \ \ ; \ \ p_k(\tau) = \frac{q_k(t)}{L}\bar{\Phi}_k\left(\frac{l_n}{L}\right) \\
&\bar{\beta}_1 = \int_0^1 \frac{\partial^4\bar{\Phi}_k}{\partial\bar{x}^4}(\bar{x})\bar{\Phi}_k(\bar{x})d\bar{x} \ \ ; \ \ \bar{\beta}_2 = \int_0^1 \bar{\Phi}_k^2(\bar{x})d\bar{x} \\
&\epsilon c = \frac{c_{NES}}{mL\omega_k} \ \ ; \ \ \epsilon C_p = \frac{C}{m\omega_k} \ \ ; \ \ \alpha = \frac{\bar{\Phi}_k^2\left(\frac{l_n}{L}\right)}{\bar{\beta}_2} \\
&\epsilon\Gamma(\tau) = \frac{L^2\bar{\Phi}_k\left(\frac{l_n}{L}\right)}{EI\bar{\beta}_1}\int_0^L f_a(x,t)\Phi_k(x)\mathrm{d}x \\
&\epsilon\bar{\mathcal{F}} : X \mapsto \frac{L^2}{EI}\frac{\bar{\beta}_2}{\bar{\beta}_1}\mathcal{F}\left(LX\right)
\end{aligned} \tag{C.1}$$

Appendix D. Matrix $\mathbb{M}$

$$\mathbb{M} = \begin{bmatrix} \mathbb{M}_{11} & \mathbb{M}_{12} \\ \mathbb{M}_{21} & \mathbb{M}_{22} \end{bmatrix} \tag{D.1}$$

$$\begin{aligned}
\mathbb{M}_{11} &= \frac{1}{2i} - \frac{c}{2} - \frac{\varphi_2\varphi_2^* G_0'(\varphi_2\varphi_2^*)}{2i} - \frac{G_0(\varphi_2\varphi_2^*)}{2i} \\
\mathbb{M}_{12} &= -\frac{\varphi_2^2 G_0'(\varphi_2\varphi_2^*)}{2i} \\
\mathbb{M}_{21} &= \frac{{\varphi_2^*}^2 G_0'(\varphi_2\varphi_2^*)}{2i} \\
\mathbb{M}_{22} &= -\frac{1}{2i} - \frac{c}{2} + \frac{\varphi_2\varphi_2^* G_0'(\varphi_2\varphi_2^*)}{2i} + \frac{G_0(\varphi_2\varphi_2^*)}{2i}
\end{aligned} \tag{D.2}$$

Appendix E. Matrix B_1 and B_2

$$B_1 = \begin{bmatrix} \frac{1}{2i} & 0 \\ 0 & -\frac{1}{2i} \end{bmatrix} \tag{E.1}$$

$$B_2 = \begin{bmatrix} b_{11} & b_{12} \\ b_{21} & b_{22} \end{bmatrix} \tag{E.2}$$

$$\begin{aligned} b_{11} &= \frac{c}{2} - \frac{1}{2i} + \frac{1}{2i}\left(\frac{\partial G_0(|\varphi_2|^2)}{\partial \varphi_2}\varphi_2 + G_0(|\varphi_2|^2)\right) \\ b_{12} &= \frac{\varphi_2}{2i}\frac{\partial G_0(|\varphi_2|^2)}{\partial \varphi_2^*} \\ b_{21} &= -\frac{\varphi_2^*}{2i}\frac{\partial G_0(|\varphi_2|^2)}{\partial \varphi_2} \\ b_{22} &= \frac{c}{2} + \frac{1}{2i} - \frac{1}{2i}\left(\frac{\partial G_0(|\varphi_2|^2)}{\partial \varphi_2^*}\varphi_2^* + G_0(|\varphi_2|^2)\right) \end{aligned} \tag{E.3}$$

References

[1] G. W. Housner, L. A. Bergman, T. K. Caughey, A. G. Chassiakos, R. O. Claus, S. F. Masri, R. E. Skelton, T. T. Soong, B. F. Spencer, J. T. P. Yao, Structural control: Past, present, and future, Journal of Engineering Mechanics 123 (9) (1997) 897–971.

[2] A. M. R. S. Y. Chu, T. T. Soong, Active, Hybrid, and Semi-active Structural Control: A Design and Implementation Handbook, John Wiley and Sons, 2005.

[3] S. Korkmaz, A review of active structural control: challenges for engineering informatics, Computers & Structures 89 (23) (2011) 2113–2132.

[4] H. Frahm, Device for damping vibrations of bodies., US Patent 989,958 (1911).

[5] J. Den Hartog, Mechanical vibrations (1956), McGrawfinll Book Company (1985).

[6] R. E. Roberson, Synthesis of a nonlinear dynamic vibration absorber, Journal of the Franklin Institute 254 (3) (1952) 205–220.

[7] E. Sevin, On the parametric excitation of pendulum-type vibration absorber, Journal of Applied Mechanics 28 (3) (1961) 330–334.

[8] R. A. Struble, J. H. Heinbockel, Resonant oscillations of a beam-pendulum system, Journal of Applied Mechanics 30 (2) (196) 181–188.

[9] R. S. Haxton, A. D. S. Barr, The autoparametric vibration absorber, Journal Manufacturing Science Engineering 94 (1) (1972) 119–125.

[10] A. Vyas, A. Bajaj, Dynamics of autoparametric vibration absorbers using multiple pendulums, Journal of Sound and Vibration 246 (1) (2001) 115–135.

[11] Y. Song, H. Sato, Y. Iwata, T. Komatsuzaki, The response of a dynamic vibration absorber system with a parametrically excited pendulum, Journal of Sound and Vibration 259 (4) (2003) 747–759.

[12] I. Yamakawa, S. Takeda, H. Kojima, Behavior of a new type dynamic vibration absorber consisting of three permanent magnets, Bulletin of JSME 20 (146) (1977) 947–954.

[13] H. Kojima, K. Nagaya, A study on the torsional dynamic vibration absorber consisting of rare-earth magnets, Bulletin of JSME 26 (214) (1983) 611–618.

[14] J. B. Hunt, J. C. Nissen, The broadband dynamic vibration absorber, Journal of Sound Vibration 83 (4) (1982) 573–578.

[15] H. J. Rice, J. R. McCraith, Practical non-linear vibration absorber design, Journal of Sound Vibration 116 (3) (1987) 545–559.

[16] O. Gendelman, L. Manevitch, A. F. Vakakis, R. M'closkey, Energy pumping in nonlinear mechanical oscillators: part i—dynamics of the underlying hamiltonian systems, J. Appl. Mech. 68 (1) (2001) 34–41.

[17] A. F. Vakakis, O. Gendelman, Energy pumping in nonlinear mechanical oscillators: part ii—resonance capture, J. Appl. Mech. 68 (1) (2001) 42–48.

[18] N. E. Wierschem, D. D. Quinn, S. A. Hubbard, M. A. Al-Shudeifat, D. M. McFarland, J. Luo, L. A. Fahnestock, B. F. Spencer, A. F. Vakakis, L. A. Bergman, Passive damping enhancement of a two-degree-of-freedom system through a strongly nonlinear two-degree-of-freedom attachment, Journal of Sound and Vibration 331 (25) (2012) 5393–5407.

[19] F. Nucera, A. F. Vakakis, D. M. McFarland, L. Bergman, G. Kerschen, Targeted energy transfers in vibro-impact oscillators for seismic mitigation, Nonlinear Dynamics 50 (3) (2007) 651–677.

[20] O. Gendelman, A. Alloni, Dynamics of forced system with vibro-impact energy sink, Journal of Sound and Vibration 358 (2015) 301–314.

[21] E. Gourc, G. Michon, S. Seguy, A. Berlioz, Targeted energy transfer under harmonic forcing with a vibro-impact nonlinear energy sink: analytical and experimental developments, Journal of Vibration and Acoustics 137 (3) (2015).

[22] E. Gourc, S. Seguy, G. Michon, A. Berlioz, B. Mann, Quenching chatter instability in turning process with a vibro-impact nonlinear energy sink, Journal of Sound and Vibration 355 (2015) 392–406.

[23] C.-H. Lamarque, O. V. Gendelman, A. Ture Savadkoohi, E. Etcheverria, Targeted energy transfer in mechanical systems by means of non-smooth nonlinear energy sink, Acta mechanica 221 (1) (2011) 175–200.

[24] O. V. Gendelman, A. F. Vakakis, L. A. Bergman, D. M. McFarland, Asymptotic analysis of passive nonlinear suppression of aeroelastic instabilities of a rigid wing in subsonic flow, SIAM Journal on Applied Mathematics 70 (5) (2010) 1655–1677.

[25] A. Ture Savadkoohi, C.-H. Lamarque, Z. Dimitrijevic, Vibratory energy exchange between a linear and a nonsmooth system in the presence of the gravity, Nonlinear Dynamics 70 (2) (2012) 1473–1483.

[26] B. Vaurigaud, L. Manevitch, C.-H. Lamarque, Passive control of aeroelastic instability in a long span bridge model prone to coupled flutter using targeted energy transfer, Journal of Sound and Vibration 330 (11) (2011) 2580–2595.

[27] B. Cochelin, P. Herzog, P.-O. Mattei, Experimental evidence of energy pumping in acoustics, Comptes Rendus Mécanique 334 (11) (2006) 639–644.

[28] A. Labetoulle, A. Ture Savadkoohi, E. Gourdon, Detection of different dynamics of two coupled oscillators including a time-dependent cubic nonlinearity, Acta Mechanica 233 (1) (2022) 259–290.

[29] P. Van Dyke, D. Havard, A. Laneville, Effect of Ice and Snow on the Dynamics of˜Transmission Line Conductors, in: M. Farzaneh (Ed.), Atmospheric Icing of Power Networks, Springer Netherlands, Dordrecht, 2008, pp. 171–228.

[30] J. P. D. Hartog, Transmission Line Vibration Due to Sleet, Transactions of the American Institute of Electrical Engineers 51 (4) (1932) 1074–1076.

[31] O. Nigol, G. Clarke, Conductor galloping and control based on torsional mechanism, IEEE 74 (1974) 016–2.

[32] P. Yu, Y. M. Desai, A. H. Shah, N. Popplewell, Three-Degree-of-Freedom Model for Galloping. Part I: Formulation, Journal of Engineering Mechanics 119 (12) (1993) 2404–2425.

[33] K. F. Jones, Coupled Vertical and Horizontal Galloping, Journal of Engineering Mechanics 118 (1) (1992) 92–107.

[34] D. Zulli, G. Piccardo, A. Luongo, On the nonlinear effects of the mean wind force on the galloping onset in shallow cables, Nonlinear Dynamics 103 (4) (2021) 3127–3148.

[35] A. Zhou, X. Liu, S. Zhang, F. Cui, P. Liu, Wind tunnel test of the influence of an interphase spacer on the galloping control of iced eight-bundled conductors, Cold Regions Science and Technology 155 (2018) 354–366.

[36] D. Havard, J. Pohlman, Five Years' Field Trials of Detuning Pendulums for Galloping Control, IEEE Transactions on Power Apparatus and Systems PAS-103 (2) (1984) 318–327.

[37] S. Langlois, F. Legeron, Prediction of aeolian vibration on transmission-line conductors using a nonlinear time history model—part i: Damper model, IEEE Transactions on Power Delivery 29 (3) (2014) 1168–1175.

[38] M. Kani, S. Khadem, M. Pashaei, M. Dardel, Vibration control of a nonlinear beam with a nonlinear energy sink, Nonlinear Dynamics 83 (1) (2016) 1–22.

[39] Z. N. Ahmadabadi, S. Khadem, Nonlinear vibration control of a cantilever beam by a nonlinear energy sink, Mechanism and Machine Theory 50 (2012) 134–149.

[40] F. Georgiades, A. Vakakis, Dynamics of a linear beam with an attached local nonlinear energy sink, Communications in Nonlinear Science and Numerical Simulation 12 (5) (2007) 643–651.

[41] O. Chabart, J.-L. Lilien, Galloping of electrical lines in wind tunnel facilities, Journal of Wind Engineering and Industrial Aerodynamics 74 (1998) 967–976.

[42] A. H. Nayfeh, Perturbation Methods, John Wiley and Sons, 2005.

[43] L. I. Manevitch, The description of localized normal modes in a chain of nonlinear coupled oscillators using complex variables, Nonlinear Dynamics 25 (1) (2001) 95–109.

[44] C. Bertrand, A. Ture Savadkoohi, V. Acary, C.-H. Lamarque, Reduced-order model for the nonlinear dynamics of cables, Journal of Engineering Mechanics 148 (9) (2022) 04022052.